Gauge Equivariant Neural Networks for Quantum Lattice Gauge Theories

Di Luo,[1,2,3,†] Giuseppe Carleo,[4] Bryan K. Clark,[1,2] and James Stokes[5,*]

[1]*Department of Physics, University of Illinois at Urbana-Champaign, Illinois 61801, USA*
[2]*IQUIST and Institute for Condensed Matter Theory and NCSA Center for Artificial Intelligence Innovation, University of Illinois at Urbana-Champaign, Illinois 61801, USA*
[3]*The NSF AI Institute for Artificial Intelligence and Fundamental Interactions, 77 Massachusetts Ave, Cambridge, Massachusetts 02139, USA*
[4]*Institute of Physics, École Polytechnique Fédérale de Lausanne (EPFL), CH-1015 Lausanne, Switzerland*
[5]*Center for Computational Quantum Physics and Center for Computational Mathematics, Flatiron Institute, New York, New York 10010, USA*

(Received 24 December 2020; accepted 11 November 2021; published 30 December 2021)

Gauge symmetries play a key role in physics appearing in areas such as quantum field theories of the fundamental particles and emergent degrees of freedom in quantum materials. Motivated by the desire to efficiently simulate many-body quantum systems with exact local gauge invariance, gauge equivariant neural-network quantum states are introduced, which exactly satisfy the local Hilbert space constraints necessary for the description of quantum lattice gauge theory with $\mathbb{Z}_d$ gauge group and non-Abelian Kitaev $D(G)$ models on different geometries. Focusing on the special case of $\mathbb{Z}_2$ gauge group on a periodically identified square lattice, the equivariant architecture is analytically shown to contain the loop-gas solution as a special case. Gauge equivariant neural-network quantum states are used in combination with variational quantum Monte Carlo to obtain compact descriptions of the ground state wave function for the $\mathbb{Z}_2$ theory away from the exactly solvable limit, and to demonstrate the confining or deconfining phase transition of the Wilson loop order parameter.

DOI: 10.1103/PhysRevLett.127.276402

Introduction.—Quantum many-body systems defined on a lattice with local gauge invariance occur ubiquitously in the description of physics at diverse energy scales—they appear in the effective theories of many-electron systems [1] and topological phases [2], in bosonization of two-dimensional lattice fermions [3,4], and in the microscopically regulated description of interacting elementary particles in the standard model [5]. Quantum lattice gauge theories are characterized by the fact that the physical states span a subspace of the many-body Hilbert space which is defined by satisfying a set of local operator constraints. These operator constraints gives rise to group invariance of the associated wave function, called gauge invariance.

Because of the analytic intractability of gauge theories, it is important to develop techniques for simulating them. Methods such as lattice-gauge theory [6] accomplish this via a quantum-classical mapping which rewrites the quantum problems as a statistical mechanics problem in one higher dimension. This mapping can only be done for sign-free problems without introducing a "negative" weight in the statistical mechanics model which induces either an exponential cost in the simulations or the need for additional approximations to mitigate the sign problem. Alternatively, quantum gauge theories can be simulated using variational methods based on compact parametrizations of many-body wave functions. DMRG [7], a variational approach based on matrix-product states, has been extensively used to analyze gauge theories [8]. While DMRG is efficacious for one-dimensional systems, the bond-dimension of the matrix product state needed to accurately represent the ground state grows exponentially with width in higher dimensions.

Machine-learning techniques based on a neural-network variational representation of quantum states [9], have extended the scope of variational methods by accurately representing low-energy states of strongly correlated systems in two or more spatial dimensions [10–18]. Imposing physical symmetries in neural-network quantum states is a very active research topic [19,20] that reflects the broader need to impose symmetries in machine learning applications to physics [21]. Our work further extends the scope of neural-network quantum states by developing gauge equivariant neural networks which are special-purpose variational families of wave functions that are explicitly gauge invariant.

Our work is inspired by recent developments of group-invariant networks with group equivariant layers. These have found applications both in data science and physics. For data science, the data-generating process is often assumed to be invariant under a symmetry group G [22,23]. For example, Ref. [24] derived equivariant layers starting from the assumption that the input data transforms covariantly as a tensor field on a Riemannian manifold. Very recently, gauge equivariant networks have been constructed and variationally optimized using the reverse-relative entropy to approximate the Gibbs distribution associated with the Euclidean action functional for lattice Yang-Mills in the case of Abelian U(1) [25] and subsequently non-Abelian SU(N) gauge group [26] (a different gauge-equivariant construction for this non-Abelian group is also considered in Ref. [27]). The approach of Refs. [25,26], which is closely related to variational inference [28], relies on the existence of an analytic continuation between the quantum theory and a positive-definite Gibbs measure, which presents a challenge in the presence of fermions, however, due to the well-known sign problem.

The Letter is organized as follows. The $\mathbb{Z}_2$ gauge theory Hamiltonian is introduced using a notation that generalizes to the $\mathbb{Z}_d$ gauge group and higher dimensional models such as the 3D toric code and X-cube model (explicitly described in the Supplemental Material [37], Secs. III and IV). The general construction of the gauge equivariant neural network is then described. Gauge equivariant neural wave functions are variationally optimized using variational Monte Carlo methods on square lattices up to system size 12×12, demonstrating the transition of Wilson loop order parameters from perimeter to area law.

$\mathbb{Z}_2$ gauge theory.—We start by briefly reviewing the formulation of the lattice gauge theory for the simplest nontrivial gauge group $\mathbb{Z}_2 = \{-1, 1\}$. The generalization to $\mathbb{Z}_d$ and higher dimensional models, such as 3D toric code and X-cube model, are discussed in Sec. III and IV of the Supplemental Material [37]. We consider the Hamiltonian with $\mathbb{Z}_2$ fields on the edges $e \in E$ of a periodic square lattice,

$$H = -J\sum_{f\in F} B_f - h\sum_{e\in E} X_e, \tag{1}$$

with $B_f \coloneqq \prod_{e\in f} Z_e$, where F is the set of the smallest 1×1 plaquettes $\square$ on the lattice, $e \in f$ are the edges around plaquette f and Z_e, X_e are the usual Pauli matrices. Let V be the set of vertices on the lattice. In order to define the Hilbert space of physical states, define a local operator for each vertex $v \in V$ consisting of the product of Pauli-X operators incident on the given vertex, $A_v \coloneqq \prod_{e\ni v} X_e$, where $e \ni v$ indicates the edges containing v. These vertex operators commute amongst themselves, commute with the Hamiltonian H and have eigenvalues ± 1. In this work we focus on the so-called even gauge theory in which the physical Hilbert space $\mathcal{H}_{\text{phys}}$ is chosen to be the $+1$ eigenspace of all vertex operators,

$$\mathcal{H}_{\text{phys}} \coloneqq \{|\psi\rangle \in \mathcal{H} : A_v|\psi\rangle = |\psi\rangle \ \ \forall \ \ v \in V\}. \tag{2}$$

Since the vertex operators satisfy the global operator identity $\prod_{v\in V} A_v = \mathbb{1}$, it follows that only $|V| - 1$ of the constraints defining $\mathcal{H}_{\text{phys}}$ are independent. The dimension of physical state space is therefore found to be $\dim \mathcal{H}_{\text{phys}} = (2^{|E|}/2^{|V|-1}) = 2^{L^2+1}$. Further details on the description of the Hilbert space are provided in Sec. I of the Supplemental Material [37].

The $\mathbb{Z}_2$ gauge theory is exactly solvable in both the weak coupling ($h \to 0$) and strong coupling ($h \to \infty$) limits. For infinite transverse field $h = \infty$ the nondegenerate ground state is simply the uniform superposition state $|+\rangle^{\otimes E}$ which is manifestly gauge invariant, where $|+\rangle$ satisfies $X|+\rangle = |+\rangle$. In the opposite extreme of $h = 0$, the ground states are also eigenstates of all B_f and are fourfold degenerate. As shown originally by Wegner using duality arguments [29], the uniform superposition $|+\rangle^{\otimes E}$ and the ground states at $h = 0$ correspond to different phases of matter, which are distinguished by the expectation value of a nonlocal operator called the Wilson loop, which is defined for any closed curve $C \subseteq E$ on the lattice as follows:

$$\hat{W}_C \coloneqq \prod_{e\in C} Z_e. \tag{3}$$

Wegner found a critical value of the transverse field h_c separating a deconfined phase for $h < h_c$ in which $\langle \hat{W}_C \rangle$ decays exponentially with the perimeter of C, from a confined phase where $\langle \hat{W}_C \rangle$ decays exponentially with the area enclosed by C.

Gauge equivariant neural networks.—We present now a neural network which explicitly preserves the gauge invariance of the wave function. The classical configuration space $\mathbb{Z}_2^E$ can be regarded as a subset of the continuous vector space $\mathbb{C}^E \coloneqq \mathbb{C}^{L\times L\times 2}$ consisting of tensors with shape $(L, L, 2)$, where the edge e is specified by the vertex $v \in V$ indexed by the first two axes and the direction $\mu \in \{\hat{x}, \hat{y}\}$ indexed by the third axis. The components of an arbitrary tensor $\phi \in \mathbb{C}^E$ will then be indexed as $\phi_\mu(v)$ where $v \in V$ and $\mu \in \{\hat{x}, \hat{y}\}$. The action of the gauge group on the space of $(L, L, 2)$ tensors is described as follows. Given a square matrix $\Omega \in \{-1, 1\}^V \coloneqq \{-1, 1\}^{L\times L}$, we define a gauge transformation $g_\Omega : \mathbb{C}^E \to \mathbb{C}^E$ by the following rule,

$$(g_\Omega \cdot \phi)_\mu(v) \coloneqq \Omega(v)\phi_\mu(v)\Omega(v + \mu), \tag{4}$$

where $\Omega(v)$ and $\Omega(v + \mu)$ denote the entries of the matrix Ω at the lattice location $v \in V$ and the shifted lattice location $v + \mu \in V$, assuming boundaries are periodically identified. It is straightforward to show that the gauge

transformation associated with Hilbert space operator A_v is given by g_{Ω_v} where Ω_v is defined for each $v' \in V$ by,

$$\Omega_v(v') = \begin{cases} -1, & v' = v \\ +1, & v' \neq v \end{cases}. \tag{5}$$

A wave function that obeys the Gauss law constraint is then one in which

$$\Psi(g_{\Omega_v} \cdot \phi) = \Psi(\phi), \tag{6}$$

for the case where $\phi \in \mathbb{Z}_2^E$. Let us call a function $h: \mathbb{C}^E \to \mathbb{C}$ gauge invariant if it satisfies $h(g_\Omega \cdot \phi) = h(\phi)$ for all g_Ω and a function $f: \mathbb{C}^E \to \mathbb{C}$ gauge equivariant if it satisfies $f(g_\Omega \cdot \phi) = g_\Omega \cdot f(\phi)$ for all g_Ω. A wave function that consists of multiple layers of gauge equivariant functions interwoven with pointwise nonlinearities followed by a final gauge invariant layer is guaranteed to obey Eq. (6) since group equivariance is preserved by composure and pointwise nonlinearities. In the following, we construct neural network blocks that are equivariant and invariant, respectively.

Gauge equivariant layer.—The construction of the gauge equivariant layer parallels the construction found in Ref. [25], applied to discrete Abelian groups. Given vertices $v, v' \in V$ and a path $\gamma \subseteq E$ from v to v', consisting of a sequence of adjacent edges, we define the Wilson path as the function $W_\gamma: \mathbb{C}^E \to \mathbb{C}$ given by the formula,

$$W_\gamma(\phi) \coloneqq \prod_{e \in \gamma} \phi_e. \tag{7}$$

It is easy to show that for any Ω and any path γ from v to v' we have

$$W_\gamma(g_\Omega \cdot \phi) = \Omega(v) W_\gamma(\phi) \Omega(v'). \tag{8}$$

The above Wilson path is the fundamental primitive from which the gauge-equivariant layers will be constructed. Note that if γ is a closed curve C then the function W_C is gauge invariant.

Consider a fixed equivariant layer described by the equivariant function $f: \mathbb{C}^E \to \mathbb{C}^E$. Each such layer is specified by decorating the edges $e = (v, v + \mu) \in E$ of the lattice with the following data: (1) A path $\gamma_e \subseteq E$ from v to $v + \mu$ (2) A collection of $n_e \geq 1$ closed curves $C_1^e, \ldots C_{n_e}^e$ (3) A parametrized neural network $h_e: \mathbb{C}^{n_e} \to \mathbb{C}$. From the above data we construct a gauge-equivariant function $f: \mathbb{C}^E \to \mathbb{C}^E$ defined for all $\phi \in \mathbb{C}^E$ by the rule $f: \phi_e \mapsto f_e(\phi)$, where

$$f_e(\phi) \coloneqq W_{\gamma_e}(\phi) h_e[W_{C_1^e}(\phi), \ldots, W_{C_{n_e}^e}(\phi)]. \tag{9}$$

The equivariance follows directly from Eq. (8). The explicit calculation is outlined below for convenience of the reader,

$$\begin{aligned} f_e(g_\Omega \cdot \phi) &= h_e[W_{C_1^e}(g_\Omega \cdot \phi), \ldots, W_{C_n^e}(g_\Omega \cdot \phi)] W_{\gamma_e}(g_\Omega \cdot \phi) \\ &= h_e[W_{C_1^e}(\phi), \ldots, W_{C_n^e}(\phi)] \Omega(v) W_{\gamma_e}(\phi) \Omega(v + \mu) \\ &= \Omega(v) f_e(\phi) \Omega(v + \mu) \end{aligned} \tag{10}$$

$$= [g_\Omega \cdot f(\phi)]_e. \tag{11}$$

Numerical experiments.—Here we determine the phase diagram of Eq. (1) for different values of the transverse field h. When $h = 0$, we can analytically write a network that exactly represents the ground state with a single gauge invariant block (and no equivariant blocks), which is detailed in Sec. II of the Supplemental Material [37]. For all h, we use variational Monte Carlo methods to approximately determine the ground states on square lattices. The family of variational wave functions is summarized graphically in Fig. 1. It consists of multiple gauge equivariant layers, in which the gauge invariant Wilson loop features within each layer were chosen to consist of all elementary plaquettes of the form $\gamma_e = \square$.

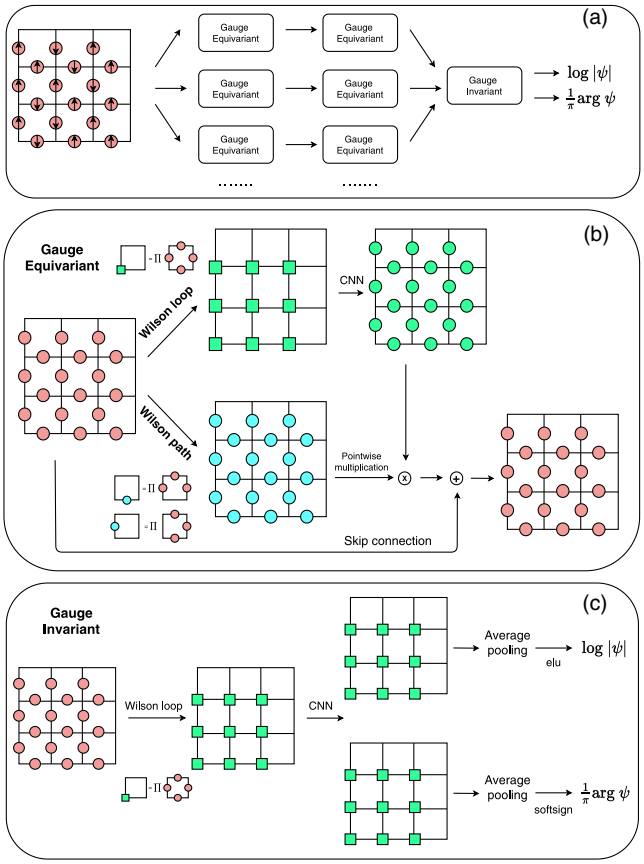

FIG. 1. (a) Gauge equivariant neural network architecture. (b) Gauge equivariant block. (c) Gauge invariant block. For (b) and (c), the convolution neural network (CNN) component uses channel = 2, stride = 1, activation function = leaky relu and periodic boundary padding. The kernel size in CNN is different for different systems sizes.

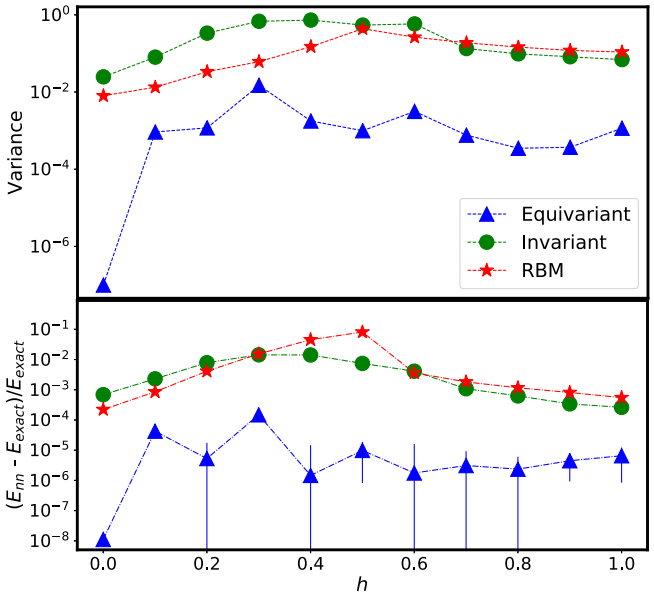

FIG. 2. The variance (top) and the energy difference between the exact ground state (bottom) of the gauge equivariant network, gauge invariant network (no equivariant layers) and RBM on a 3×3 lattice of Eq. (1). The details of the above networks are provided in Sec. VI of the Supplemental Material [37].

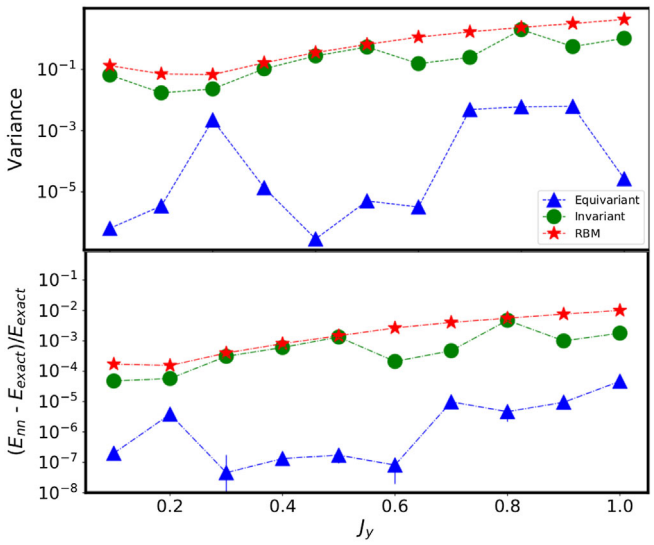

FIG. 3. The variance (top) and the energy difference between the exact ground state (bottom) of the gauge equivariant network, gauge invariant network (no equivariant layers) and RBM on a 3×3 lattice of $H = -\sum_{f\in F}\prod_{e\in f} Z_e - \sum_{e\in E} X_e - J_y \sum_{f\in F}\prod_{e\in f} Y_e$. The details of the above networks are the same as Fig. 2.

The gauge equivariant Wilson path associated with each edge e is chosen to be the curves of the form $\sqcap$ and $\sqsubset$ ending on e. Real-valued weights and biases are used in all neural networks. The neural networks h_e are chosen to be convolutional neural network with periodic padding to capture symmetry and facilitate transfer learning. Residual layers or equivalently skip connections, which are manifestly gauge equivariant, are also employed. The neural network parameters are optimized using the stochastic reconfiguration algorithm [30]. Further details about the architecture and optimization are provided in Sec. V of the Supplemental Material [37].

We start with a benchmark of the Hamiltonian in Eq. (1) on a 3×3 square lattice by comparing gauge equivariant neural network, gauge invariant network, restricted Boltzmann machine (RBM) and exact diagonalization, where Fig. 2 presents the energy and variance. In addition, we benchmark a Hamiltonian with a sign problem $H = -J\sum_{f\in F}\prod_{e\in f} Z_e - h\sum_{e\in E} X_e - J_y \sum_{f\in F}\prod_{e\in f} Y_e$ for $J = h = 1$, which results are shown in Fig. 3. The number of variational parameters for the above three neural networks are 66, 24, and 1044, respectively. It can be seen that even with small number of parameters, the gauge equivariant neural network achieves better performance than the RBM and attains accurate results close to the exact. We further apply our method to larger square lattices of size $L \times L$ with $L \in \{8, 10, 12\}$. It is known that the Wilson loop expectation value $\langle \hat{W}_C \rangle$ decays exponentially with area law for $h > h_c$ and with perimeter law for $h < h_c$ [31].

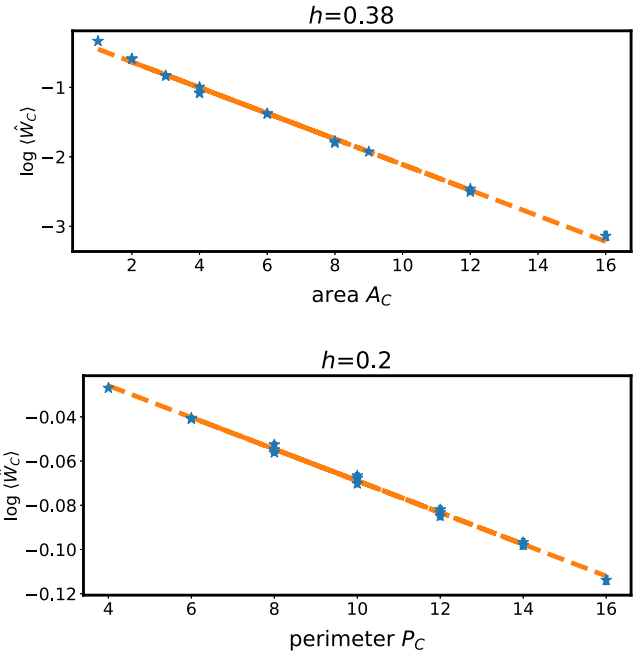

FIG. 4. The ground state expectation value of rectangle Wilson loops of size $l_1 \times l_2$ ($l_1, l_2 \leq 4$) as a function of the enclosed area A_C in the confining phase for $h > h_c$ (top) and of the enclosed perimeter P_C in the deconfined phase for $h < h_c$ (bottom) on a 12×12 lattice. The linear fit to the log-linear plot is consistent with area law scaling $\langle \hat{W}_C \rangle \sim e^{-\alpha A_C}$ with best fit parameter $\alpha = 0.185$ and a perimeter law scaling $\langle \hat{W}_C \rangle \sim e^{-\alpha' P_C}$ with best fit parameter $\alpha' = 0.00718$. Because of the smallness of α', we note that a linear fit of $\langle \hat{W}_C \rangle$ versus P_C is also consistent with the data.

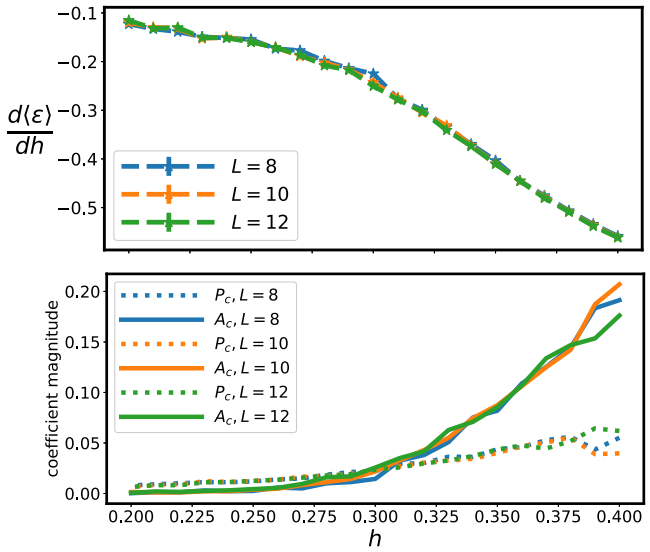

FIG. 5. Based on the optimized gauge equivariant states on $L \times L$ lattices as a function of h, it shows (top) derivative of the energy per site calculated by the Hellmann-Feynman theorem. (Bottom) Magnitude of k_1 (solid) and k_2 (dotted) for fitting $\log\langle\hat{W}_C\rangle = k_1 A_C + k_2 P_C + b$ with area A_c and perimeter P_c. The changes at around $h = 0.30$ in the top figure and the increase in A_c in the bottom figure suggest the confined or deconfined phase transition.

In Fig. 4, the variational wave function is shown to capture the area law and the perimeter law behaviors of the Wilson loop in the corresponding regimes and attains the related decay factors. In Fig. 5, we compute the energy derivatives and perform a simultaneous fitting of area and perimeter law for $\log\langle\hat{W}_C\rangle$ with different h. The changes of the data at around $h = 0.3$ suggest a deconfinement or confinement phase transition, which is consistent with Refs. [32,33].

Discussion and future directions.—In this work, we have showed how to use gauge equivariant networks to represent variational states which exactly obey local gauge constraints. This significantly expands the space of models whose phase diagrams can now be numerically established. For example, one could variationally explore the phase diagrams of the $\mathbb{Z}_d$ lattice gauge theory for $d > 2$ (see the Supplemental Material [37], Sec. III); the 3D toric code (Sec. IV of Ref. [37]); X-cube fracton model (Sec. IV of Ref. [37]) or Kitave $D(G)$ models (Sec. V of Ref. [37]) with external field; or models with disorder. Another interesting application would be to relax the restriction to the even sector of the gauge theory and explore the physics of different gauge sectors. Beyond the explicit constructions given here, it will be interesting to further extend the reach of such networks by generalizing the approach described in this work to models with different gauge symmetries or constraints from gauging subsystem symmetries. Finally, the ability to exactly employ gauge constraints variationally has the potential to have impact beyond ground state calculations, for example, in overcoming obstacles in optimizing combinatorial structures [34] or in successful quantum-state tomography [35].

Di Luo acknowledges helpful discussion with Jiayu Shen, Luke Yeo, Oleg Dubinkin, Ryan Levy, Peijun Xiao, and Ruoyu Sun. We acknowledge support from the Department of Energy Grant No. DOE de-sc0020165. The work is partially done with intern and computational support from the Center for Computational Mathematics at the Flatiron Institute. G. C. is supported by the Swiss National Science Foundation under Grant No. 200021_200336. The numerical experiments were conducted using NetKet [36].

*Corresponding author.
jstokes@flatironinstitute.org
†diluo2@illinois.edu

[1] P. A. Lee, N. Nagaosa, and X.-G. Wen, Rev. Mod. Phys. **78**, 17 (2006).
[2] A. Kitaev and C. Laumann, arXiv:0904.2771.
[3] Y.-A. Chen, A. Kapustin, and D. Radicevic, Ann. Phys. (Amsterdam) **393**, 234 (2018).
[4] S. B. Bravyi and A. Y. Kitaev, Ann. Phys. (Amsterdam) **298**, 210 (2002).
[5] J. Kogut and L. Susskind, Phys. Rev. D **11**, 395 (1975).
[6] J. B. Kogut, Rev. Mod. Phys. **51**, 659 (1979).
[7] S. R. White, Phys. Rev. Lett. **69**, 2863 (1992).
[8] M. C. Bañuls and K. Cichy, Rep. Prog. Phys. **83**, 024401 (2020), publisher: IOP Publishing.
[9] G. Carleo and M. Troyer, Science **355**, 602 (2017).
[10] D. Luo and B. K. Clark, Phys. Rev. Lett. **122**, 226401 (2019).
[11] D. Pfau, J. S. Spencer, A. G. D. G. Matthews, and W. M. C. Foulkes, Phys. Rev. Research **2**, 033429 (2020).
[12] J. Hermann, Z. Schätzle, and F. Noé, Nat. Chem. **12**, 891 (2020).
[13] M. Hibat-Allah, M. Ganahl, L. E. Hayward, R. G. Melko, and J. Carrasquilla, Phys. Rev. Research **2**, 023358 (2020).
[14] J. Stokes, J. R. Moreno, E. A. Pnevmatikakis, and G. Carleo, Phys. Rev. B **102**, 205122 (2020).
[15] O. Sharir, Y. Levine, N. Wies, G. Carleo, and A. Shashua, Phys. Rev. Lett. **124**, 020503 (2020).
[16] S. Lu, X. Gao, and L.-M. Duan, Phys. Rev. B **99**, 155136 (2019).
[17] X. Gao and L.-M. Duan, Nat. Commun. **8**, 662 (2017).
[18] I. Glasser, N. Pancotti, M. August, I. D. Rodriguez, and J. I. Cirac, Phys. Rev. X **8**, 011006 (2018).
[19] K. Choo, G. Carleo, N. Regnault, and T. Neupert, Phys. Rev. Lett. **121**, 167204 (2018).
[20] T. Vieijra, C. Casert, J. Nys, W. De Neve, J. Haegeman, J. Ryckebusch, and F. Verstraete, Phys. Rev. Lett. **124**, 097201 (2020).
[21] G. Carleo, I. Cirac, K. Cranmer, L. Daudet, M. Schuld, N. Tishby, L. Vogt-Maranto, and L. Zdeborová, Rev. Mod. Phys. **91**, 045002 (2019).

[22] T. Cohen and M. Welling, in *Proceedings of the International Conference on Machine Learning* (2016), pp. 2990–2999.
[23] R. Kondor and S. Trivedi, in *Proceedings of the International Conference on Machine Learning* (2018), pp. 2747–2755.
[24] T. S. Cohen, M. Weiler, B. Kicanaoglu, and M. Welling, arXiv:1902.04615.
[25] G. Kanwar, M. S. Albergo, D. Boyda, K. Cranmer, D. C. Hackett, S. Racanière, D. J. Rezende, and P. E. Shanahan, Phys. Rev. Lett. **125**, 121601 (2020).
[26] D. Boyda, G. Kanwar, S. Racanière, D. J. Rezende, M. S. Albergo, K. Cranmer, D. C. Hackett, and P. E. Shanahan, Phys. Rev. D **103**, 074504 (2021).
[27] M. Favoni, A. Ipp, D. I. Müller, and D. Schuh, arXiv:2012.12901.
[28] D. M. Blei, A. Kucukelbir, and J. D. McAuliffe, J. Am. Stat. Assoc. **112**, 859 (2017).
[29] F. J. Wegner, J. Math. Phys. (N.Y.) **12**, 2259 (1971).
[30] F. Becca and S. Sorella, *Quantum Monte Carlo Approaches for Correlated Systems* (Cambridge University Press, Cambridge, England, 2017).
[31] K. Gregor, D. A. Huse, R. Moessner, and S. L. Sondhi, New J. Phys. **13**, 025009 (2011).
[32] J. Vidal, S. Dusuel, and K. P. Schmidt, Phys. Rev. B **79**, 033109 (2009).
[33] F. Wu, Y. Deng, and N. Prokof'ev, Phys. Rev. B **85**, 195104 (2012).
[34] S. Shalev-Shwartz, O. Shamir, and S. Shammah, arXiv:1703.07950.
[35] G. Torlai, G. Mazzola, J. Carrasquilla, M. Troyer, R. Melko, and G. Carleo, Nat. Phys. **14**, 447 (2018).
[36] G. Carleo, K. Choo, D. Hofmann, J. E. T. Smith, T. Westerhout, F. Alet, E. J. Davis, S. Efthymiou, I. Glasser, S.-H. Lin, M. Mauri, G. Mazzola, C. B. Mendl, E. van Nieuwenburg, O. O'Reilly, H. Théveniaut, G. Torlai, F. Vicentini, and A. Wietek, SoftwareX **10**, 100311 (2019).
[37] See Supplemental Material at http://link.aps.org/supplemental/10.1103/PhysRevLett.127.276402 for exact constructions of toric code ground states, generalizations to other lattice gauge theories, additional numerical details.